Preparation of Nickel-Impregnated Activated Carbon Catalyst and Its Application in Co-gasification of Municipal Solid Waste and Coconut Shell

Imron Rosyadi*‡, Yusvardi Yusuf*, Nuryoto**, Suyitno***, Zainal Arifin***, Tata Sutardi ****, Kurniawan Putra Yudha*

*Department of Mechanical Engineering, Faculty of Engineering, Universitas Sultan Ageng Tirtayasa, Indonesia

**Department of Chemical Engineering, Faculty of Engineering, Universitas Sultan Ageng Tirtayasa, Indonesia

***Department of Mechanical Engineering, Faculty of Engineering, Universitas Sebelas Maret (UNS), Indonesia

**** Research Centre for Energy Conversion and Conservation, BRIN, Indonesia

(imron_jtm@untirta.ac.id (I.R.), yusvardi.untirta@gmail.com (Y.Y.), nuryoto@untirta.ac.id (N.), suyitno@staff.uns.ac.id (S.), zainal_arifin@staff.uns.ac.id (Z.A), tata012@brin.go.id (T.S), wawannitro@gmail.com (K.P.Y.))

‡ Corresponding Author; Imron Rosyadi, Department of Mechanical Engineering, Faculty of Engineering, Universitas Sultan Ageng Tirtayasa, Cilegon, 42435, Indonesesia, Telp : +6285219639360 , imron_jtm@untirta.ac.id

Received: 03.11.2023 Accepted:13.12.2023

Abstract- The abundant municipal solid waste (MSW) and coconut shells can be overcome with gasification technology. The type of catalyst can affect the gasification process significantly. The purposes of this study were to prepare nickel-impregnated activated carbon catalysts and utilize them in the co-gasification of MSW and coconut shells. First, carbon was prepared through pyrolysis of coconut shells at 450°C. Then, the carbon was activated using KOH and neutralized with 1M HCl. Furthermore, it was calcinated at various temperatures of 550, 650, and 750°C. The resulting activated carbon was impregnated using nickel ($Ni(NO_3)_2 \cdot 6H_2O$) at various stirring temperatures (50 and 90°C) with or without a holding time (for 24 hours after stirring). Characterization of catalysts was conducted using BET, XRD, SEM-EDS, and gas chromatography tests. The results showed that the best calcination temperature was 650°C, resulting in activated carbon with the highest BET surface area of 1253 m^2/g and iodine absorption capacity of 984 mg/g. Furthermore, the optimum conditions in the impregnation process were a stirring temperature of 50°C with a holding time of 24 hours, resulting in the best nickel-impregnated activated carbon catalyst (with code ACNi50D). XRD test showed that crystals of Ni and NiO elements were well visible in the ACNi50D catalyst. SEM-EDS test showed that there was a good distribution of Nickel (Ni), Oxygen (O), and Carbon (C) elements in the ACNi50D catalyst. In the co-gasification process test, the ACNi50D catalyst resulted in syngas with higher H_2 content (58%) compared to the other catalysts.

Keywords Activated Carbon, Catalyst, Gasification, Nickel, Syngas.

1. Introduction

Over the last few decades, the demand for renewable energy has continued to increase because of the increasingly depleted and limited availability of fossil energy. Through government regulation number 22 of 2017, the Indonesian government has a target to increase new and renewable energy (NRE) consumption to at least 23% of total energy in 2025 and at least 31% of total energy in 2050, but nowday in 2022 only 15% [1]. Therefore, nowadays, research on new

and renewable energy production is very important in Indonesia

Renewable energy can be generated through a gasification process. This process is attractive because it can convert waste into clean energy. It is better than conventional combustion methods which result in high pollutant emissions (such as CO_2, SO_x, and NO_x) [2],[3]. Gasification is the process of converting carbon into syngas thermochemically through a partial oxidation reaction with gasifying agents such as steam, air, CO_2, oxygen, or a combination of them [4],[5],[6]. Biomass and coal gasification reactions generally occur at high temperatures (550–1600°C) [7], [8]. The largest gas fractions in syngas are N_2, CO, H_2, and CO_2. Meanwhile, the gasification process also results in other products, namely tar and char [9]–[13].

In the gasification process, tar can be converted into lighter gases through thermal cracking at a specific residence period at high temperatures. An increase in temperature increases the tar amount. The maximum biomass tar amount is reached at around 773 K. However, at temperatures above 873 K, tar cracking occurs, so the tar is converted to non-condensable gas, thereby increasing the gas energy content [14].

Catalysts can speed up the reaction rate and aid tar cracking and catalytic reforming in the gasification process [15]–[23]. Catalyst types can be categorized into two, namely synthetic and natural catalysts. Synthetic catalysts are more widely used in industry but they are very expensive. On the other hand, natural catalysts have a cheaper price [24]–[27]. One of the natural catalysts is activated carbon. Activated carbon has a wider surface area and higher porosity than non-activated carbon. The surface area of non-activated carbon is below 300 m^2/g [28], [29], while that of biomass-based activated carbon is above 300 m^2/g [30], [31], then that of commercial activated carbon is above 400 m^2/g [32],[33],[34]. However, currently, the utilization of biomass-based activated carbon as a catalyst material in gasification is not widely used.

Carbon activation can be done via 2 methods. The first method is chemical activation with alkali metal hydroxides, carbonate salts, chlorides, sulfates, and alkaline earth phosphates [35], [36], [37], inorganic acids such as H_2SO_4, and H_3PO_4 [38], [39], [40], [41] and inorganic alkalis such as KOH and NaOH [42], [31], [34]. The second method is physical activation, which is the process of breaking the carbon chain of organic compounds through heating at a temperature of 500-900°C [31]. The chemical activation method is more attractive than the other methods because it produces activated carbon with a larger surface area [31],[43].

In the chemical activation process, there is a calcination stage. The calcination process can increase the thermal resistance of the material [44]. Generally, calcination is employed to create thermodynamically stable mixed metal oxides by thermally reacting simple metal oxide powders [45]. Calcination temperature is one of the affecting factors, that greatly affects the amounts and physicochemical characteristics of bulk density and surface area of activated carbon [30]. An increase in calcination temperature can increase the development of micropore structures, but at a temperature of 800°C, micropores will collapse and turn into mesopores [46]. An important characteristic of activated carbon is surface area. The surface area is directly proportional to the level of adsorption on organic compounds [47]. Therefore, research to determine the optimum calcination temperature in preparing biomass-based activated carbon catalysts needs to be carried out with temperature variations below 800°C.

The performance of activated carbon as a catalyst can be improved through the impregnation process. Impregnation is the process of filling a porous absorbent material with a liquid or viscous product. A previous study by Sitthikhankaew et al. reported that the impregnation of activated carbon using KOH alkaline media at room temperature can enhance the ability of the activated carbon to adsorb H_2S [34]. Furthermore, Septiawati et al. studied the impregnation of activated carbon with nickel (II) chloride and the utilization of the modified catalyst to convert benzene into cyclohexane [48].

Precious metal catalysts (such as Pt, Ru, Rh, Ir, and Pd) can be used as impregnating agents. The precious metals Rh and Pt show the highest catalytic activity, but these metals have small reservations and are expensive [49], [50]. Meanwhile, nickel catalysts are known to have high efficiency in breaking down hydrocarbon bonds and decomposing tar. In addition, nickel has a cheaper price and greater regeneration availability than precious metals [51], so nickel is considered an impregnated agent in this study.

Temperature and stirring time are affecting factors in the catalyst impregnation process. Several previous studies carried out impregnation using nickel metal (from $Ni(NO_3)_2{\cdot}6H_2O$) in several buffer media such as zeolite (natural or synthetic), CaO, and Al_2O_3 with stirring temperatures and times of 60-80°C and 1-24 hours, respectively [51], [52], [53]. However, the impregnation of biomass-based activated carbon using $Ni(NO_3)_2{\cdot}6H_2O$ is still limited.

Based on the information above, the current study aimed to investigate the impact of calcination temperature in the activation stage as well as stirring temperature and holding time (after stirring) in the impregnation stage on the characteristics of the nickel-impregnated activated carbon catalysts. Then, the resulting catalysts were used in the co-gasification process of mixed biomass of municipal solid waste (MSW) and coconut shells to produce syngas. MSW and coconut shells are abundant in Indonesia country. Indonesia is the largest coconut producer in the world, spread across a series of islands in the Indian and Pacific oceans with a 17 million metric ton production capacity [54]. Coconut shells can serve as biomass feedstock which is capable of producing high heating value of fuel and fixed carbon [55].

The co-gasification of MSW and biomass has the potential to be a more promising technology, its ability to deliver increased electrical efficiency, maintain stable operation of gasification plants, and ensure a more reliable

supply of raw materials., stable operation of gasification plants, and ensure a more reliable supply of raw materials [56].

2. Materials and Methods

2.1. Materials

MSW was collected from Serang City, Banten Province, Indonesia. Coconut shells were obtained from traditional markets located in Serang City, Banten Province, Indonesia. Chemicals of KOH and HCl were obtained from Merck, and $Ni(NO_3)_2{\cdot}6H_2O$ was obtained from PT. Smart Lab Indonesia.

2.2. Preparation of Catalyst

2.2.1. Preparation of activated carbon

Coconut shells were crushed, ground, and sifted to get biomass with 40 mesh size. Then they were heated using an induction heating furnace at 450°C for 2 hours. Then, the resulting carbon was crushed, ground, and sifted to get carbon with 18 mesh size. Next, the carbon as much as 50 g was soaked in a concentrated potassium hydroxide (KOH) solution with a mass ratio of carbon:KOH of 1:4 g/g, then stirred for 1 hour at room conditions. After that, the mixture was stored in a closed container for 24 hours. Then, 1M HCl solution was used to wash the carbon until it reached pH 7. Next, the carbon at 110°C for 12 hours using an oven. Furthermore, the carbon is calcined at various temperatures of 550, 650, and 750°C for 1 hour. The resulting activated carbons were labeled AC550, AC650, and AC750, respectively.

2.2.2. Preparation of nickel-impregnated activated carbon

The best-activated carbon produced in section 2.2.1 was then used in this section. First, about 33.76 g $Ni(NO_3)_2{\cdot}6H_2O$ was added to 100 mL of water. It was mixed using a magnetic stirrer for 30 minutes until homogeneous. Next, 50 g of activated carbon was added to the solution. After that, it was stirred for 2 hours at various temperatures of 50 and 90°C. Then, the mixture was stored in a closed container for 24 hours (holding time). After that, the catalyst was dried at 120°C for 8 hours. Next, calcination was carried out at 700°C for 2 hours [57]. Experiment details in this section are shown in Table 1.

Table 1. Experiments on making Nickel-Impregnated Activated Carbon

Code	Stirring temperature (°C)	Stirring time + holding time
ACNi50	50	2 hours
ACNi50D	50	2 hours + 24 hours
ACNi90	90	2 hours
ACNi90D	90	2 hours + 24 hours

2.3. Characterization of Catalyst

The Brunauer–Emmett–Teller (BET) test was carried out using the BET Surface Area Quantachrome Nova 4200e instrument to determine the surface area of catalysts (the activated carbon and the nickel-impregnated activated carbon). The Barret-Joyner-Halenda (BJH) method was employed to study the distribution of pore size of the catalysts. The iodine adsorption test was conducted to measure the capability of activated carbon to adsorb iodine. The X-ray diffraction (XRD) test was run using the D2Phaser XRD instrument from Bruker to study the structure and composition of the nickel-impregnated activated carbon catalysts. XRD testing was carried out at 2θ with intensity in the range of 10° – 90°. The microstructure of the nickel-impregnated activated carbon catalysts was assessed using the Phenom ProX Scanning Electron Microscope (SEM) instrument fitted with the Energy Dispersive X-ray Spectroscopy (EDS) capability.

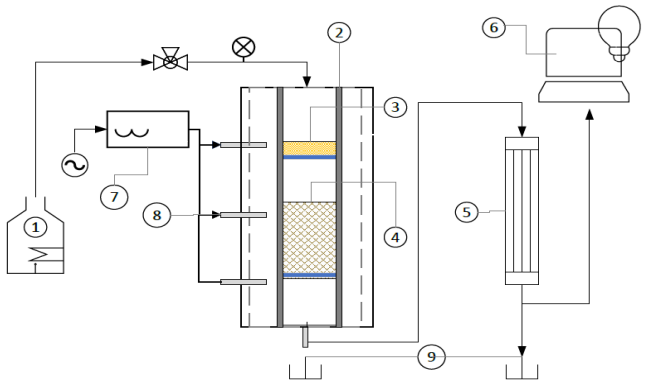
2.4. Gasification

The gasification process was run using a fixed bed reactor with an induction heater and a programmed temperature controller. The reactor tube consists of 2 parts (the bottom and the top). The biomass was placed in the bottom part and the nickel-impregnated activated carbon catalyst was placed in the top part. The biomass consisted of MSW and coconut shells. The coconut shells were obtained from traditional markets in the city of Serang, Banten Province, Indonesia. They were crushed to get a size of about 5×5 mm. Meanwhile, MSW was obtained from Serang City, Banten Province, Indonesia with a fixed composition and then dried at 120°C for 8 hours before being mixed with the coconut shells. The MSW and coconut shells were mixed with a mass ratio of 1:1 g/g.

The biomass was put in the bottom part of the tube and the catalyst was put in the top part of the tube and supported by K wool Ceramic Fiber material (High-Temperature Insulating Material up to 1260°C). The catalyst-to-biomass ratio was 1:5 g/g. The reactor was electrically heated with three K-type thermocouples monitoring the temperatures of the furnace, actual biomass, and actual catalyst, respectively. After the gasification reaction temperature was stable, the steam was fed to the gasification zone with a ratio of steam:biomass of 1.3. The integration of the water-gas shift (WGS) reaction was identified to transform CO into H_2 and CO_2 [58]. The co-gasification temperature was adjusted to 700°CThe catalyst in the decomposition process enables the reaction to occur within a relatively moderate temperature range of 600 to 900 [59]. Activated carbon can be applied across a in a wide temperature range, around 250 to 800 ºC [60]. Therefore, this study used a gasification temperature of 700ºC. Figure 1 shows the detailed experimental setup for the co-gasification process.

The gas (H_2, CO, CH_4, CO_2) resulting from the gasification process was collected and analyzed using a Gas chromatography instrument (Agilent GC 7820A) to determine its content. The instrument consisted of an Ultimetal HayesepQ T 80/100 mesh column used to measure

the concentrations of H_2, CO, and CH_4, and an Ultimetal Hayesep T 80/100 column used to determine the concentrations of CO_2 and C1-C4 hydrocarbons. The helium gas was used as a carrier gas.



1. Evaporator
2. Reactor
3. Catalyst
4. Biomass
5. Condenser
6. GC-MS
7. Panel control
8. Thermocouple
9. Tar

Fig. 1. Experimental setup for co-gasification experiment.

3. Results and Discussion

3.1. Physicochemical Properties of Activated Carbon

3.1.1. Surface area, pore volume, pore diameter, and iodine adsorption capacity

In preparing the activated carbon, the calcination temperatures were varied to 550, 650, and 750°C. The resulting activated carbon was characterized. The surface area, pore volume, pore diameter, and iodine adsorption capacity of the resulting activated carbon are shown in Table 2.

Table 2. Physicochemical properties of the activated carbon

Code	Surface area (m^2/g)	Pore volume (cc/g)	Pore diameter (nm)	Iodine adsorption capacity (mg/g)
AC550	890	0.27	4.1	792
AC650	1253	0.56	4.6	984
AC750	1017	0.43	5.3	926

An increase in calcination temperature from 550 to 650°C increased the surface area from 890 to 1253 m^2/g. However, further increasing the calcination temperature from 650 to 750°C decreased the surface area from 1253 to 1017 m^2/g. An increase in surface area is correlated with an increase in pore volume and iodine adsorption capacity (up to 24%).

At temperatures above 650°C, oxidation activity might begin to occur and change the micropore structures into mesopore structures [61]. Hence, the activated catalyst generated at a calcination temperature of 750°C might have higher mesopore and lower micropore amounts than that at a calcination temperature of 650°C. The iodine adsorption capability is attributed to the large numbers of micropores present, giving capillary action which results in high adsorption power. According to Khalil [62], at temperatures above 700°C, KOH can encourage oxidation so activated carbon production decreases. Activated Carbon with a large pore diameter size and surface area can provide a good place for adsorbents or impregnating agents [63].

3.1.2. XRD analysis

The diffraction patterns of activated carbons are presented in Figure 2. Based on Figure 2, activated carbons have very irregular microcrystalline structures where the graphite microcrystals are randomly oriented.

The poor crystallinity of all activated carbons produced at different calcination temperatures results in nearly no diffraction peaks being found. Some peaks are found randomly and asymmetrically. This shows that there are no other compounds that can be traced by X-rays. In Figure 2, the highest peak is found in the 2θ range of 24-26°. The finding of this study is consistent with that of a previous study reporting that diffraction peaks of a graphite sample are quite broad and are found in the 2θ range of 15-30º [64]

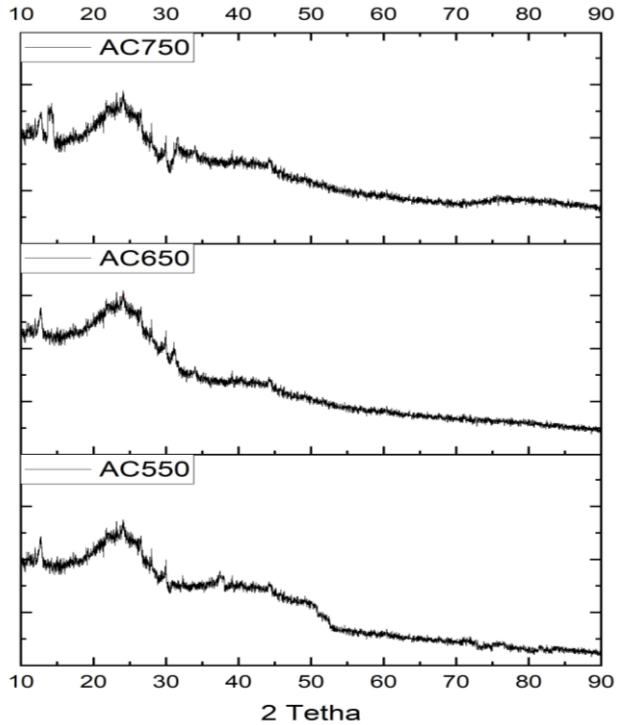


Fig. 2. XRD diffraction patterns of activated carbons.

3.2. Physicochemical Properties of Nickel-Impregnated Activated Carbon

3.2.1. Surface area, pore volume, and pore diameter

The physicochemical properties of nickel-impregnated activated carbon catalysts are shown in Table 3. The catalysts with a stirring temperature of 90ºC (ACNi90 and ACNi90D) had a lower surface area than the catalyst with a stirring temperature of 50ºC (ACNi50 and ACNi50D). The ACNi90 had the lowest surface area (146.5 m^2/g) and the ACNi90D had a surface area of 237.4 m^2/g. Furthermore, the ACNi50 had a surface area of 462.5 m^2/g, while the ACNi90D had a surface area of 584.6 m^2/g. It showed that an increase in stirring temperature from 50 to 90ºC decreased the surface area of the catalysts. Then, the existing holding time for 24 hours increased the surface area of the catalysts.

Furthermore, in general, increasing the stirring temperature from 50 to 90ºC decreased the pore volume (Table 3). The ACNi50D catalyst had a higher pore volume than the ACNi50 catalyst, namely 0.61 and 0.52 cm^3/g, respectively. This phenomenon showed that a holding time of 24 hours can increase the pore volume of the catalyst.

Table 3. Physicochemical properties of the nickel-impregnated activated catalysts

	Surface area (m^2/g)	Pore volume (cm^3/g)	Pore diameter (nm)
ACNi50	462.5	0.52	15.71
ACNi50D	584.6	0.61	13.86
ACNi90	146.5	0.54	24.43
ACNi90D	237.4	0.47	18.24

3.2.2. XRD analysis

Moreover, the stirring temperature from 50 to 90ºC increased pore diameter (Table 3). The ACNi90 catalyst had a higher pore diameter, namely 24.43 nm, compared to the ACNi50 catalyst, namely 15.71 nm. Then, holding time for 24 hours decreased pore diameter. However, the pore diameter of all catalysts was still within a reasonable tolerance. In this impregnation treatment, the pore diameter size was in the range of 10-30 nm, which was a very favorable size for the adsorbents [65].

The crystal phase in nickel-impregnated activated carbon catalysts was identified through XRD analysis and the results can be seen in Figure 3. From Figure 3, the peak at around 26.62º in the ACNi50 and ACNi50D samples is identified as the reflection plane of carbon element [31], [66]. However, in the ACNi90 and ACNi90D samples, the peak at this angle is not clearly visible. The ACNi90 and ACNi90D catalysts had a relatively larger pore diameter (see Table 3), so their active carbon lattice might be filled with nickel. The small pore diameter with wide distribution reduces the migration of solutes during material impregnation [67].

Nickel is a metal with a face-centered-cubic (FCC) crystal structure. According to the literature, the planes (111), (200), and (220) in the face-centered-cubic (FCC) structure of nickel metal (JCPDS 87-0712) are responsible for the intense diffraction peaks at approximately 44.5º, 51.8º, and 76.4º [68], [69]. In this study, diffraction peaks for Ni can be identified at 2θ angles of 44.52°, 51.77° and 76.32° in the ACNi50D, ACNi90 and ACNi90D catalysts, respectively. Based on the literature, the diffraction peaks at around 37.14º, 43.19º, and 62.87º are attributed to the (111), (200), and (220) planes of the face-centered cubic phase of NiO (JCPDS 04-0835) [68], [70].

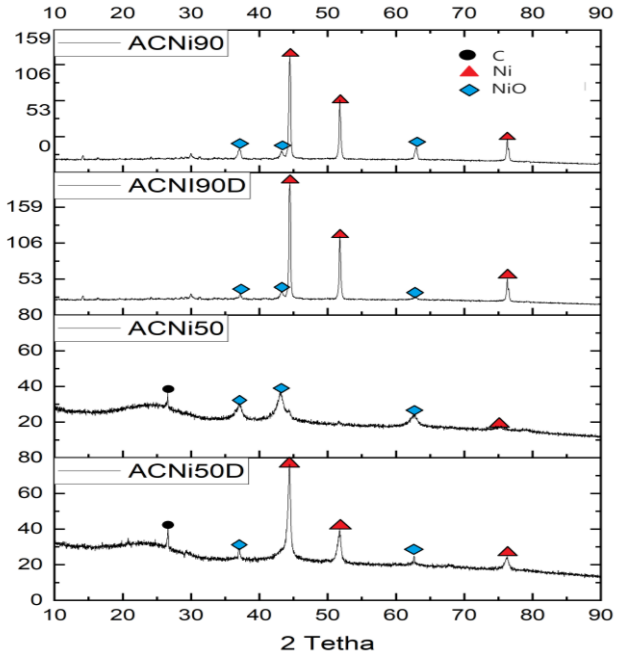


Fig. 3. XRD diffraction patterns of nickel-impregnated activated carbon catalysts.

In this study, the NiO diffraction peaks were visible in the ACNi50 catalyst, but the Ni diffraction peaks in the ACNi50 catalyst were weak. In ACNi50, the presence of Ni crystals was not identified, this was possible because the Ni in the catalyst had reacted with oxygen to form NiO [71]. In the ACNi90 and ACNi90D, there were diffraction peaks for the elements Ni and NiO. The Ni diffraction peaks in the ACNi50 and ACNi50D catalysts appeared weaker and lower than those in the ACNi90 and ACNi90D catalysts. This shows that increasing the temperature can increase the crystal structure of Ni (see Figure 3) but decrease the surface area (see Table 3). In the ACNi50D catalyst, the Ni peak appears very clearly and the NiO appears very weak at around 37.5º and 62.34º. This shows that in this catalyst, NiO was weakened and reduced well.

3.3. Syngas Production

The co-gasification process with mixed biomass of MSW and coconut shells with a mass ratio of 50:50 was carried out using various catalysts (ACNi50, ACNi50D, ACNi90, and ACNi90D). The composition of the resulting syngas is shown in Figure 4. The NiAC50D catalyst resulted in syngas with the highest energy content because the syngas contained the highest hydrogen content, namely 58% (Figure 4). This was because the NiAC50D catalyst had a higher

surface area than other catalysts (Table 3). In steam reforming, with metal-based catalysts, steam reacts with methane to form CO and H_2 under the temperature of 700 to 1100°C [72].

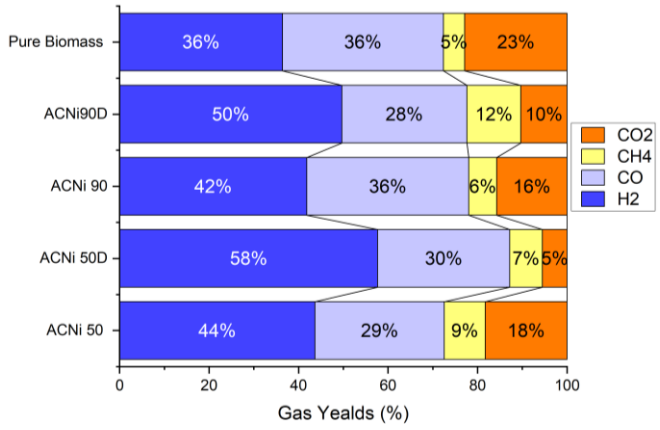


Fig. 4. Composition of syngas resulting from gasification using nickel-impregnated activated carbon catalysts.

The nickel-impregnated activated carbon catalysts have a crystal structure of Ni and NiO which synergize with each other, thereby resulting in a good catalytic ability. Based on Figure 4, comprehensively, the nickel-impregnated activated carbon catalysts produced syngas with H_2, CO, CH_4, and CO_2 contents in the range of 42-58%, 28-36%, 6-12%, and 5-18%. On the other hand, gasification without a catalyst (pure biomass) resulted in syngas H_2, CO, CH_4, and CO_2 content of 36%, 36%, 5%, and 23%, respectively. It shows that gasification without a catalyst resulted in lower H_2 and CH_4 contents and higher CO and CO_2 contents than that with the catalysts. It means that the use of nickel-impregnated activated carbon catalysts had a positive effect on the quality of syngas products. In this study, the production of H_2 is notably dominant compared to other types of gases. This is considered a positive aspect, given that the current production cost of H_2 is known to be relatively high [73].

3.4. SEM-EDS Mapping Analysis

Based on sub-section 3.3, the best catalyst was ACNi50D. Therefore, the morphology of the ACNi50D catalyst was analyzed using SEM. Figure 5 shows the SEM-EDS Mapping analysis results. Based on Figure 5, the ACNi50D catalyst has a fairly good crystal structure. The elements of Nickel (Ni) and oxygen (O) are evenly visible (Figure 5). Based on the XRD test results (Figure 3), the ACNi50D catalyst has more prominent NiO contents compared to other catalysts. In this catalyst, carbon also appears evenly distributed (see Figure 5) as support for Ni/NiO. This is also supported by the XRD test results which show very clear carbon diffraction in this catalyst. Thus, the ACNi50D catalyst contained a good combination of activated carbon and Ni/NiO, so it had good performance in the gasification process in producing syngas with the highest H_2 content (Figure 4).

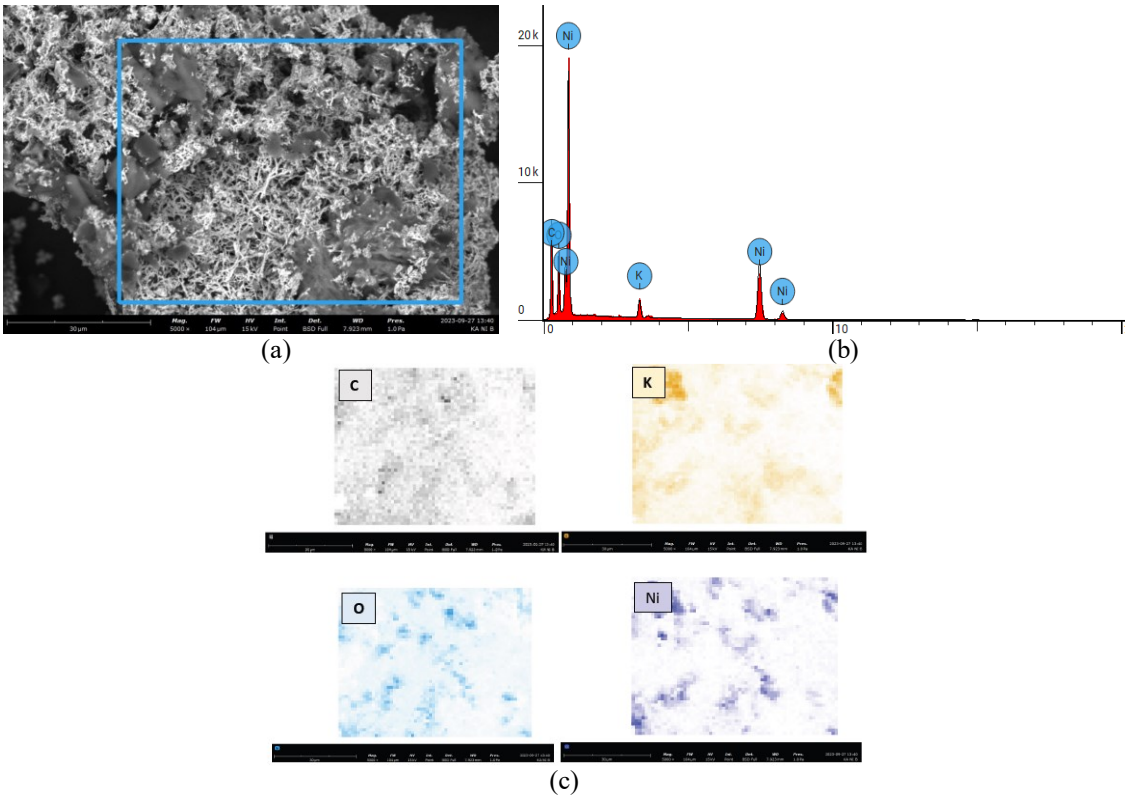


Fig. 5. SEM-EDS Mapping of ACNi50D catalyst: (a) SEM result, (b) EDS result, (c) Mapping result. Remarks = C is carbon, K = potassium, O = Oxygen, Ni = Nickel.

4. Conclusion

The production of activated carbon from coconut shells was conducted at various calcination temperatures of 550, 650, and 750ºC. The results showed that the calcination temperature of 650ºC was the best because it produced a catalyst with the highest surface area with good iodine adsorption. Then, the best-activated carbon was impregnated using nickel with variations of stirring temperatures of 50 and 90ºC with or without holding time for 24 hours. The best nickel-impregnated activated carbon catalyst was the ACNi50D catalyst obtained at a stirring temperature of 50ºC with a holding time of 24 hours. According to the XRD analysis, the catalyst contained crystal structures of Ni and NiO well visible. The gasification process using the ACNi50D catalyst produced syngas with the highest H_2 content, namely 58%. In the ACNi50D catalyst, activated carbon elements can be seen with an amorphous structure. Based on SEM-EDS analysis, the Nickel (Ni), Oxygen (O), and Carbon (C) were evenly distributed in the catalyst. The ACNi50D catalyst had the highest surface area, namely 584.6 m^2/g, which can be used as a supported medium for Ni and NiO metal catalysts and an ion exchange medium.

Acknowledgment

The author would like to thank the Directorate of Research and Community Service (DP2M), Directorate General of Higher Education (DIKTI) for supporting research funding (research grant number 0557/E5.5/AL.04/2023). Many thanks to all those who have assisted in finishing this research.

References

[1] F. Vianda and R. Y. Wirawan, "Indonesia Energy Transition Outlook 2022," Institute for Essential Services Reform (IESR), 2022. https://iesr.or.id/wp-content/uploads/2022/01/Indonesia-Energy-Transition-Outlook-2022-IESR-Digital-Version-.pdf (accessed Oct. 27, 2023).

[2] A. Ramos, E. Monteiro, V. Silva, and A. Rouboa, "Co-gasification and recent developments on waste-to-energy conversion: A review," Renewable and Sustainable Energy Reviews, vol. 81. Elsevier Ltd, pp. 380–398, 2018. doi: 10.1016/j.rser.2017.07.025.

[3] A. Akhtar, V. Krepl, and T. Ivanova, "A combined overview of combustion, pyrolysis, and gasification of biomass," Energy and Fuels, vol. 32, no. 7, pp. 7294–7318, 2018, doi: 10.1021/acs.energyfuels.8b01678.

[4] J. M. Bermudez and B. Fidalgo, Production of bio-syngas and bio-hydrogen via gasification. 2016. doi: 10.1016/B978-0-08-100455-5.00015-1.

[5] P. Bajpai, Biomass conversion processes. 2020. doi: 10.1016/b978-0-12-818400-4.00005-0.

[6] P. Basu, Gasification Theory. Elsevier Inc., 2013. doi: 10.1016/b978-0-12-396488-5.00007-1.

[7] J. Eshun, L. Wang, E. Ansah, A. Shahbazi, K. Schimmel, V. Kabadi, S. Aravamudhan, "Characterization of the physicochemical and structural evolution of biomass particles during combined pyrolysis and CO2 gasification," J. Energy Inst., vol. 92, no. 1, pp. 82–93, 2019, doi: 10.1016/j.joei.2017.11.003.

[8] X. Yao, Q. Liu, Z. Kang, Z. An, H. Zhou, and K. Xu, "Quantitative study on thermal conversion behaviours and gas emission properties of biomass in nitrogen and in CO2/N2 mixtures by TGA/DTG and a fixed-bed tube furnace," Energy, vol. 270, no. February, p. 126904, 2023, doi: 10.1016/j.energy.2023.126904.

[9] C. Li and K. Suzuki, "Tar property, analysis, reforming mechanism and model for biomass gasification-An overview," Renew. Sustain. Energy Rev., vol. 13, no. 3, pp. 594–604, 2009, doi: 10.1016/j.rser.2008.01.009.

[10] T. Kan, V. Strezov, and T. J. Evans, "Lignocellulosic biomass pyrolysis: A review of product properties and effects of pyrolysis parameters," Renew. Sustain. Energy Rev., vol. 57, pp. 1126–1140, 2016, doi: 10.1016/j.rser.2015.12.185.

[11] Z. A. B. Z. Alauddin, P. Lahijani, M. Mohammadi, and A. R. Mohamed, "Gasification of lignocellulosic biomass in fluidized beds for renewable energy development: A review," Renew. Sustain. Energy Rev., vol. 14, no. 9, pp. 2852–2862, 2010, doi: 10.1016/j.rser.2010.07.026.

[12] D. Feng, Y. Zhao, Y. Zhang, Z. Zhang, L. Zhang, and S. Sun, "In-situ steam reforming of biomass tar over sawdust biochar in mild catalytic temperature," Biomass and Bioenergy, vol. 107, no. November, pp. 261–270, 2017, doi: 10.1016/j.biombioe.2017.10.007.

[13] X. Kan, X. Chen, Y. Shen, A. A. Lapkin, M. Kraft, and C. H. Wang, "Box-Behnken design based CO2 co-gasification of horticultural waste and sewage sludge with addition of ash from waste as catalyst," Appl. Energy, vol. 242, no. February, pp. 1549–1561, 2019, doi: 10.1016/j.apenergy.2019.03.176.

[14] L. Fagbemi, L. Khezami, and R. Capart, "Pyrolysis products from different biomasses: Application to the thermal cracking of tar," Appl. Energy, vol. 69, no. 4, pp. 293–306, 2001, doi: 10.1016/S0306-2619(01)00013-7.

[15] Y. K. Choi, J. H. Ko, and J. S. Kim, "A new type three-stage gasification of dried sewage sludge: Effects of equivalence ratio, weight ratio of activated carbon to feed, and feed rate on gas composition and tar, NH3, and H2S removal and results of approximately 5 h gasification," Energy, vol. 118, pp. 139–146, 2017, doi: 10.1016/j.energy.2016.12.032.

[16] C. Font Palma, "Modelling of tar formation and evolution for biomass gasification: A review," Applied Energy, vol. 111. Elsevier Ltd, pp. 129–141, 2013. doi: 10.1016/j.apenergy.2013.04.082.

[17] R. S. Tan, T. A. Tuan Abdullah, S. A. Mahmud, R. Md Zin, and K. Md Isa, "Catalytic steam reforming of

complex gasified biomass tar model toward hydrogen over dolomite promoted nickel catalysts," Int. J. Hydrogen Energy, vol. 44, no. 39, pp. 21303–21314, 2019, doi: 10.1016/j.ijhydene.2019.06.125.

[18] J. Chen, K. Zhao, Z. Zhao, F. He, Z. Huang, and G. Wei, "Identifying the roles of MFe2O4 (M=Cu, Ba, Ni, and Co) in the chemical looping reforming of char, pyrolysis gas and tar resulting from biomass pyrolysis," Int. J. Hydrogen Energy, vol. 44, no. 10, pp. 4674–4687, 2019, doi: https://doi.org/10.1016/j.ijhydene.2018.12.216.

[19] P. Ammendola, E. Cammisa, R. Chirone, L. Lisi, and G. Ruoppolo, "Effect of sulphur on the performance of Rh-LaCoO3 based catalyst for tar conversion to syngas," Appl. Catal. B Environ., vol. 113–114, pp. 11–18, 2012, doi: 10.1016/j.apcatb.2011.07.024.

[20] M. Irfan, A. Li, L. Zhang, M. Javid, M. Wang, and S. Khushk, "Enhanced H2 production from municipal solid waste gasification using Ni-CaO-TiO2 Bifunctional catalyst prepared by dc arc plasma melting," Ind. Eng. Chem. Res., vol. 58, no. 29, pp. 13408–13419, 2019, doi: 10.1021/acs.iecr.9b01999.

[21] X. Wang, Y. He, T. Xu, B. Xiao, S. Liu, Z. Hu, J. Li, "CO2 sorption-enhanced steam reforming of phenol using Ni–M/CaO–Ca12Al14O33 (M = Cu, Co, and Ce) as catalytic sorbents," Chem. Eng. J., vol. 393, p. 124769, 2020, doi: https://doi.org/10.1016/j.cej.2020.124769.

[22] M. Shah and P. Mondal, "Optimization of CO2 reforming of methane process for the syngas production over Ni–Ce/TiO2–ZrO2 catalyst using the Taguchi method," Int. J. Hydrogen Energy, vol. 46, no. 44, pp. 22799–22812, 2021, doi: 10.1016/j.ijhydene.2021.04.091.

[23] I. Hita, T. Cordero-Lanzac, G. Bonura, C. Cannilla, J .M. Arandes, F. Frusteri, J. Bilbao, "Hydrodeoxygenation of raw bio-oil towards platform chemicals over FeMoP/zeolite catalysts," J. Ind. Eng. Chem., vol. 80, pp. 392–400, 2019, doi: 10.1016/j.jiec.2019.08.019.

[24] M. Guisnet, "Influence of zeolite composition on catalytic activity," pp. 55–67, 2007, doi: 10.1039/9781847551962-00055.

[25] M. Krol, "Natural vs. Synthetic Zeolites," Crystals, vol. 10, no. 622, pp. 1–8, 2020.

[26] L. Wei, W. Haije, N. Kumar, J. Peltonen, M. Peurla, H. Grenman, W. de Jong, "Influence of nickel precursors on the properties and performance of Ni impregnated zeolite 5A and 13X catalysts in CO2 methanation," Catal. Today, vol. 362, no. November 2019, pp. 35–46, 2021, doi: 10.1016/j.cattod.2020.05.025.

[27] A. T. N. Fajar, F. A. Nurdin, R. R. Mukti, Subagjo, C. B. Rasrendra, and G. T. M. Kadja, "Synergistic effect of dealumination and ceria impregnation to the catalytic properties of MOR zeolite," Mater. Today Chem., vol. 17, p. 100313, 2020, doi: 10.1016/j.mtchem.2020.100313.

[28] M. Tripathi, A. Bhatnagar, N. M. Mubarak, J. N. Sahu, and P. Ganesan, "RSM optimization of microwave pyrolysis parameters to produce OPS char with high yield and large BET surface area," Fuel, vol. 277, no. December 2019, p. 118184, 2020, doi: 10.1016/j.fuel.2020.118184.

[29] K. Qian, A. Kumar, K. Patil, D. Bellmer, D. Wang, W. Yuan, "Effects of biomass feedstocks and gasification conditions on the physiochemical properties of char," Energies, vol. 6, no. 8, pp. 3972–3986, 2013, doi: 10.3390/en6083972.

[30] M. E. Irem Okman, Selhan Karagoz, Turgay Tay, "Activated carbon from grape seeds by chemical activation with potassium carbonate and potassium hydroxide," Appl. Surf. Sci., 2014.

[31] E. P. N. Lingeswarran Muniandy, Farook Adam, Abdul Rahman Mohamed, "The synthesis and characterization of high purity mixed microporous/mesoporous activated carbon from risk husk using chemical activation with NaOH and KOH," Microporous Mesoporous Mater., pp. 316–323, 2014.

[32] K. Anoop Krishnan, K. G. Sreejalekshmi, and R. S. Baiju, "Nickel(II) adsorption onto biomass based activated carbon obtained from sugarcane bagasse pith," Bioresour. Technol., vol. 102, no. 22, pp. 10239–10247, 2011, doi: 10.1016/j.biortech.2011.08.069.

[33] C. R. A. de Abreu, P. Simon, R. Wojcieszak, P. M. de Souza, and F. S. Toniolo, "Effect of rhenium on the catalytic activity of activated carbon-supported nickel applied in the hydrogenation of furfural and levulinic acid," Top. Catal., vol. 65, no. 7–8, pp. 902–914, 2022, doi: 10.1007/s11244-022-01605-6.

[34] R. Sitthikhankaew, D. Chadwick, S. Assabumrungrat, and N. Laosiripojana, "Effect of KI and KOH impregnations over activated carbon on H2S Adsorption performance at low and high temperatures," Sep. Sci. Technol., vol. 49, no. 3, pp. 354–366, 2014, doi: 10.1080/01496395.2013.841240.

[35] C. I. Portela, T. R. Brazil, T. A. P. Mendonça, E. B. Santos, R. A. Domingues, N. C. S. Vieira, M. Gonçalves, "Activated carbon obtained from coffee husk waste activated by CaCl2 as support of TiO2 for the enhanced photocatalytic degradation of Victoria Blue B dye," Diam. Relat. Mater., vol. 139, no. April, p. 110417, 2023, doi: 10.1016/j.diamond.2023.110417.

[36] M. Paalo, M. Härmas, T. Romann, A. Jänes, and E. Lust, "Modification of micro/mesoporous carbon synthesis method from well decomposed peat using ZnCl2 additional activation step," Electrochem. commun., vol. 153, no. June, pp. 0–5, 2023, doi: 10.1016/j.elecom.2023.107543.

[37] A. N. Mohd Faizal, N. N. Meskam, N. R. Putra, A. S. Zaini, N. Mohamed Rusli, and M. A. Ahmad Zaini, "Preparation of beeswax residue-ZnCl2-activated

carbon for adsorption of methylene blue," Mater. Today Proc., no. August 2023, 2023, doi: 10.1016/j.matpr.2023.08.345.

[38] Y. A. B. Neolaka, Y. Lawa, J. Naat, A. A. P. Riwu, H. Darmokoesoemo, B. A. Widyaningrum, M. Iqbal, H. S. Kusuma, "Indonesian Kesambi wood (Schleichera oleosa) activated with pyrolysis and H2SO4 combination methods to produce mesoporous activated carbon for Pb(II) adsorption from aqueous solution," Environ. Technol. Innov., vol. 24, p. 101997, 2021, doi: 10.1016/j.eti.2021.101997.

[39] S. Meshram, R. S. Thakur, G. Jyoti, C. Thakur, and A. B. Soni, "Optimization of lead adsorption from lead-acid battery recycling unit wastewater using H2SO4 modified activated carbon," J. Indian Chem. Soc., vol. 99, no. 6, p. 100469, 2022, doi: 10.1016/j.jics.2022.100469.

[40] H. M. Al-swaidan and A. Ahmad, "Synthesis and characterization of activated carbon from saudi arabian dates tree ' s fronds wastes," 3rd Int. Conf. Chem. Biol. Environ. Eng., vol. 20, no. October, pp. 25–31, 2011.

[41] E. Taer, N. Yanti, A. Apriwandi, A. Ismardi, and R. Taslim, "Novel O, P, S self-doped with 3D hierarchy porous carbon from aromatic agricultural waste via H3PO4 activation for supercapacitor electrodes," Diam. Relat. Mater., vol. 140, no. PA, p. 110415, 2023, doi: 10.1016/j.diamond.2023.110415.

[42] H. P. S. Abdul Khalil, M. Jawaid, P. Firoozian, U. Rashid, A. Islam, and H. M. Akil, "Activated carbon from various agricultural wastes by chemical activation with KOH: Preparation and characterization," J. Biobased Mater. Bioenergy, vol. 7, no. 6, pp. 708–714, 2013, doi: 10.1166/jbmb.2013.1379.

[43] M. L. Sekirifa, M. Hadj-Mahammed, S. Pallier, L. Baameur, D. Richard, and A. H. Al-Dujaili, "Preparation and characterization of an activated carbon from a date stones variety by physical activation with carbon dioxide," J. Anal. Appl. Pyrolysis, vol. 99, pp. 155–160, 2013, doi: 10.1016/j.jaap.2012.10.007.

[44] B. Kaur and S. N. Bhattacharya, Automotive dyes and pigments. Woodhead Publishing Limited, 2011. doi: 10.1533/9780857094919.2.231.

[45] G. L. Messing, "Calcination and Phase Transformations," M. B. T.-E. of M. T. C. and G. Pomeroy, Ed. Oxford: Elsevier, 2021, pp. 83–92. doi: https://doi.org/10.1016/B978-0-12-818542-1.00038-2.

[46] D. W. Li, T. F. Ma, Y. Y. Tian, X. F. Zhu, and Y. Y. Qiao, "Effects of alkali/char ratio and activation temperature on ultramicropores of rice husk active carbon," Wuji Cailiao Xuebao/Journal Inorg. Mater., vol. 30, no. 1, pp. 17–22, 2015, doi: 10.15541/jim20140251.

[47] X. T. Qiongfen Yu, Ming Li, Honhong Yi, "Preparation and phosphine adsorption of activated carbon prepared from walnut shells by KOH chemical activation," Sep. Sci. Technol., 2015.

[48] E. Septiawati, "Preparation of nickeuactive carboncatalyst and it's utilization for benzene hydrogenation," Indones. J. Chem., vol. 1, no. 2, 2001, doi: https://doi.org/10.22146/ijc.21951.

[49] U. Izquierdo, V. L. Barrio, K. Bizkarra, A. M. Gutierrezb, J. R. Arraibi, L. Gartzia, J. Bañuelos, I. Lopez-Arbeloa, J. F. Cambra, "Ni and RhNi catalysts supported on Zeolites L for hydrogen and syngas production by biogas reforming processes," Chem. Eng. J., vol. 238, pp. 178–188, 2014, doi: 10.1016/j.cej.2013.08.093.

[50] L. Lyu, M. Shengene, Q. Ma, J. Sun, X. Gao, H. Fan, J. Zhang, T. S. Zhao, "Synergy of macro-meso bimodal pore and Ni-Co alloy for enhanced stability in dry reforming of methane," Fuel, vol. 310, no. PB, p. 122375, 2022, doi: 10.1016/j.fuel.2021.122375.

[51] V. Zsinka, N. Miskolczi, T. Juzsakova, and M. Jakab, "Pyrolysis-gasification of biomass using nickel modified catalysts: The effect of the catalyst regeneration on the product properties," J. Energy Inst., vol. 105, no. July, pp. 16–24, 2022, doi: 10.1016/j.joei.2022.08.003.

[52] J. Ashok, S. Naveen Kumar, M. Subrahmanyam, and A. Venugopal, "Production of COX free hydrogen by catalytic decomposition of methane over Ni/HY catalysts," Catal. Letters, vol. 118, no. 1–2, pp. 139–145, 2007, doi: 10.1007/s10562-007-9170-1.

[53] D. Yao, H. Yang, H. Chen, and P. T. Williams, "Investigation of nickel-impregnated zeolite catalysts for hydrogen/syngas production from the catalytic reforming of waste polyethylene," Appl. Catal. B Environ., vol. 227, no. July 2017, pp. 477–487, 2018, doi: 10.1016/j.apcatb.2018.01.050.

[54] Shane, "Coconut Production by Country 2023," world population review, 2023. https://worldpopulationreview.com/country-rankings/coconut-production-by-country (accessed Oct. 17, 2023).

[55] S. Salim and A. I. Tolago, "Use of Coconut Shell Become an Alternative Electricity," Int. J. Smart grid, vol. 7, no. V7i3, 2023, doi: 10.20508/ijsmartgrid.v7i3.302.g295.

[56] N. Vitkov, "Safety based comparison of incineration and gasification technologies for electrical energy production by municipal solid waste in Bulgaria," 2019 11th Electr. Eng. Fac. Conf. BulEF 2019, pp. 1–5, 2019, doi: 10.1109/BulEF48056.2019.9030788.

[57] W. Wang, C. Duong-Viet, L. Truong-Phuoc, J. M. Nhut, L. Vidal, and C. Pham-Huu, "Activated carbon supported nickel catalyst for selective CO2 hydrogenation to synthetic methane under contactless induction heating," Catal. Today, vol. 418, no. November 2022, p. 114073, 2023, doi: 10.1016/j.cattod.2023.114073.

[58] N. Slavu, C. Dinca, and C. K. Banica, "Production of H2-rich syngas from biomass gasification with CO2

capture technology," in 2021 10th International Conference on ENERGY and ENVIRONMENT (CIEM), 2021, pp. 1–5. doi: 10.1109/CIEM52821.2021.9614907.

[59] M. Msheik, S. Rodat, and S. Abanades, "Methane cracking for hydrogen production: A review of catalytic and molten media pyrolysis," Energies, vol. 14, no. 11, 2021, doi: 10.3390/en14113107.

[60] G. Ravenni, O. H. Elhami, J. Ahrenfeldt, U. B. Henriksen, and Y. Neubauer, "Adsorption and decomposition of tar model compounds over the surface of gasification char and active carbon within the temperature range 250–800 °C," Appl. Energy, vol. 241, pp. 139–151, 2019, doi: 10.1016/j.apenergy.2019.03.032.

[61] S. E. Abechi, C. E. Gimba, A. Uzairu, and Y. A. Dallatu, "Preparation and characterization of activated carbon from palm kernel shell by chemical activation," Indones. J. Chem., vol. 3, no. 7, pp. 54–61, 2013.

[62] H. P. S. Abdul Khalil, P. Firoozian, I. O. Bakare, H. M. Akil, and A. M. Noor, "Exploring biomass based carbon black as filler in epoxy composites: Flexural and thermal properties," Mater. Des., vol. 31, no. 7, pp. 3419–3425, 2010, doi: 10.1016/j.matdes.2010.01.044.

[63] V. Toteva, K. Ruskova, and A. Zahariev, "Preparation and characterization of activated carbon derived from lignocellulosic waste biomass," in 2020 III International Conference on High Technology for Sustainable Development (HiTech), 2020, pp. 1–4. doi: 10.1109/HiTech51434.2020.9363971.

[64] P. Kalyani and A. Anitha, "Refuse derived energy - tea derived boric acid activated carbon as an electrode material for electrochemical capacitors," Port. Electrochim. Acta, vol. 31, no. 3, pp. 165–174, 2013, doi: 10.4152/pea.201303165.

[65] F. Slag, Materials The Effects of Temperature on the Hydrothermal Synthesis of Hydroxyapatite-Zeolite Using Blast Furnace Slag," 2019.

[66] N. K. Kalagatur, K. Karthick, J. A. Allen, O. S. N. Ghosh, S. Chandranayaka, V. K. GuptaVijai, K. Krishna, V. Mudili, "Application of activated carbon derived from seed shells of Jatropha curcas for decontamination of zearalenone mycotoxin," Front. Pharmacol., vol. 8, no. OCT, 2017, doi: 10.3389/fphar.2017.00760.

[67] M. Börnhorst, P. Walzel, A. Rahimi, A. Kharaghani, E. Tsotsas, N. Nestle, A. Besser, F. Kleine Jäger, T. Metzger, "Influence of pore structure and impregnation–drying conditions on the solid distribution in porous support materials," Dry. Technol., vol. 34, no. 16, pp. 1964–1978, 2016, doi: 10.1080/07373937.2016.1147048.

[68] H. Xin, W. Zhou, K. Zhou, X. Du, D. Li, and C. Hu, "Controlling the growth of activated carbon supported nickel phosphide catalysts via adjustment of surface group distribution for hydrodeoxygenation of palmitic acid," Catal. Today, vol. 319, no. February 2018, pp. 182–190, 2019, doi: 10.1016/j.cattod.2018.03.051.

[69] L. A. García-Cerda, K. M. Bernal-Ramos, S. M. Montemayor, M. A. Quevedo-López, R. Betancourt-Galindo, and D. Bueno-Báques, "Preparation of hcp and fcc Ni and Ni/NiO nanoparticles using a citric acid assisted Pechini-type method," J. Nanomater., vol. 2011, 2011, doi: 10.1155/2011/162495.

[70] H. Wang, J. Han, Z. Bo, L. Qin, Y. Wang, and F. Yu, "Non-thermal plasma enhanced dry reforming of CH4 with CO2 over activated carbon supported Ni catalysts," Mol. Catal., vol. 475, no. June, 2019, doi: 10.1016/j.mcat.2019.110486.

[71] A. E. N. N. Greenwood, Chemistry of the Elements (Second Edition), 2nd editio. Elsevier, 1997. doi: 10.1016/B978-0-7506-3365-9.50033-X.

[72] A. Chanthakett, M. T. Arif, M. M. K. Khan, and A. M. T. Oo, "Chapter 8 - Hydrogen production from municipal solid waste (MSW) for cleaner environment," A. K. Azad and M. M. K. B. T.-B. R. and T. Khan, Eds. Academic Press, 2021, pp. 219–247. doi: https://doi.org/10.1016/B978-0-12-822525-7.00017-2.

[73] G. Ala, I. Colak, G. Di Filippo, R. Miceli, P. Romano, G. Schettino, C. Silva, S. Valtchev, F. Viola, "Forecasts on the development of Hydrogen Refuelling Infrastructures in Portugal," in 2021 9th International Conference on Smart Grid (icSmartGrid), 2021, pp. 112–117. doi: 10.1109/icSmartGrid52357.2021.9551212.